




## Enhancing ductility in bulk metallic glasses by straining during cooling

Rodrigo Miguel Ojeda Mota<sup>1,6</sup>, Ethen Thomas Lund <sup>1,6</sup>, Sungwoo Sohn<sup>1</sup>, David John Browne <sup>2</sup>, Douglas Clayton Hofmann<sup>3</sup>, Stefano Curtarolo<sup>4</sup>, Axel van de Walle<sup>5</sup> & Jan Schroers <sup>1</sup>✉

Most of the known bulk metallic glasses lack sufficient ductility or toughness when fabricated under conditions resulting in bulk glass formation. To address this major shortcoming, processing techniques to improve ductility that mechanically affect the glass have been developed, however it remains unclear for which metallic glass formers they work and by how much. Instead of manipulating the glass state, we show here that an applied strain rate can excite the liquid, and simultaneous cooling results in freezing of the excited liquid into a glass with a higher fictive temperature. Microscopically, straining causes the structure to dilate, hence “pulls” the structure energetically up the potential energy landscape. Upon further cooling, the resulting excited liquid freezes into an excited glass that exhibits enhanced ductility. We use  $Zr_{44}Ti_{11}Cu_{10}Ni_{10}Be_{25}$  as an example alloy to pull bulk metallic glasses through this excited liquid cooling method, which can lead to tripling of the bending ductility.

<sup>1</sup>Department of Mechanical Engineering and Materials Science, Yale University, New Haven, CT, USA. <sup>2</sup>School of Mechanical and Materials Engineering, University College Dublin, Dublin, Ireland. <sup>3</sup>Department of Applied Physics and Materials Science, California Institute of Technology, Pasadena, CA, USA. <sup>4</sup>Materials Science, Electrical Engineering, Physics and Chemistry, Duke University, Durham, NC, USA. <sup>5</sup>School of Engineering, Brown University, Providence, RI, USA. <sup>6</sup>These authors contributed equally: Rodrigo Miguel Ojeda Mota, Ethen Thomas Lund. ✉email: [jan.schroers@yale.edu](mailto:jan.schroers@yale.edu)

When a metallic glass forming liquid is cooled, its structure continuously reconfigures into a new temperature dependent metastable equilibrium structure. Such reconfiguration, referred to as structural relaxation, proceeds with a characteristic time,  $\tau_{\text{rel}}$  that rapidly increases with decreasing temperature. Reconfiguration occurs as long as the required time scale for relaxation exceeds the available time, which is usually set by the cooling rate,  $R$ ;  $\tau_{\text{cool}} = 1/R$ . However, at a certain temperature, usually referred to as the fictive temperature ( $T_f$ ) or glass transition temperature upon cooling, the metastable liquid can no longer find its metastable equilibrium and freezes into a glass. For metallic glasses, it has been generally observed that higher fictive temperatures result in higher ductility of the corresponding amorphous structure<sup>1–6</sup>.

Realizing a higher  $T_f$  and hence a ductile state in a glass upon cooling requires either a slower relaxation process or faster cooling. As the relaxation process of a BMG forming liquid is an alloy specific and intrinsic property, only the cooling rate can act as a tool to enhance ductility. As a consequence, ductile states can generally only be realized in thin and simple geometries where sufficiently high cooling rates can be achieved<sup>5</sup>, and most BMGs in bulk form lack ductility or fracture toughness<sup>7–9</sup>.

Recognizing such limitations in realizing a ductile state under BMG forming conditions has led to the development of processing strategies to enhance ductility after the glass has already been formed. Such strategies are based on mechanical means<sup>10</sup> and include irradiation<sup>11–15</sup>, static loading<sup>16–20</sup>, cyclic loading<sup>21</sup>, shot peening<sup>22</sup>, rolling<sup>23</sup>, twin roll casting<sup>24</sup>, thermal cycling<sup>25–28</sup>, and

severe plastic deformation<sup>29,30</sup>. A summary of previous results can be found in the Supplementary Table 1. Among these methods addressing the glass are some that offer practical methods to enhance ductility in BMG forming alloys<sup>25</sup>. However, it is unclear for which BMGs these techniques lead to rejuvenation or relaxation and hence a more ductile or brittle behavior, respectively<sup>27</sup>. Beyond cooling rate, other strategies that directly affect the liquid prior to glass formation have been explored but remain inconclusive<sup>31</sup>.

Here, we strain the supercooled liquid BMG former during cooling. The resulting excited liquid originates from the evolving competition between structural relaxation and strain rejuvenation. Upon freezing into a glass, the temperature at which the excited liquid state has been resumed is the representative fictive temperature of the resulting excited glass. The extent to which straining enhances the fictive temperature depends on the difference between the time scales set by the strain rate, which increases the potential energy, and by structural relaxation, which decreases the potential energy. An increase in fictive temperature is reflected in an increase in ductility which we measure in bending.

## Results

Initially amorphous  $\text{Zr}_{44}\text{Ti}_{11}\text{Ni}_{10}\text{Cu}_{10}\text{Be}_{25}$  rods of  $\sim 1.8$  mm in diameter are heated to a temperature 80 K above the calorimetric glass transition temperature ( $T_g = 623$  K). Subsequently, the sample is air cooled whilst simultaneously applying a load of 1–100 N which rapidly strains the sample, and by varying the load, the strain rate can be manipulated (Fig. 1). The decreasing

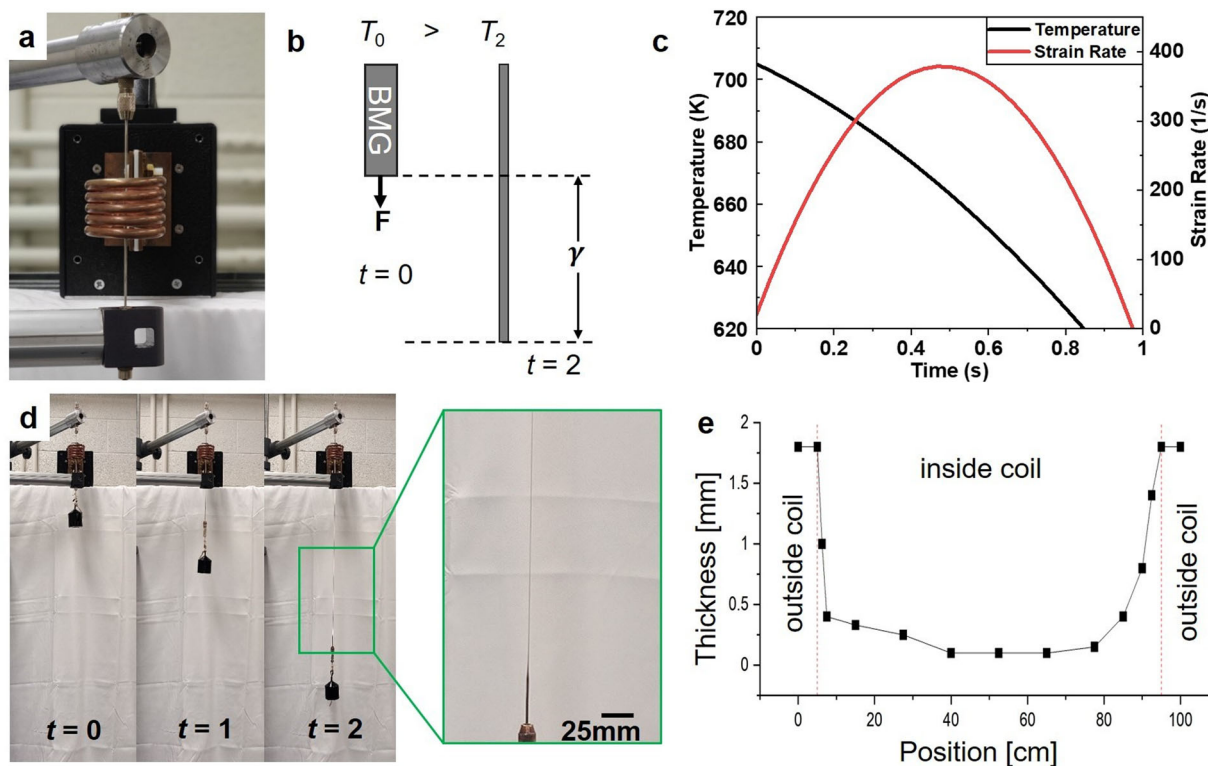


**Fig. 1 Experimental realization of excited liquid cooling.** **a** Induction heating is used to heat a BMG rod to a desired temperature in the supercooled liquid region. **b** A constant force, which can vary between 1 and 100 N, is applied to strain the sample. Upon straining, the sample is air cooled with a varying cooling rate ranging  $\sim 10$ – $100$  K/s. The variation of the cooling rate originates from the decreasing diameter of the sample upon straining from initially  $\sim 1.8$  mm to a final  $\sim 0.1$  mm. Strain,  $\gamma$ , is calculated from the sample's initial length,  $L_0$  and length at time,  $L(t)$ , by  $\gamma(t) = ((L(t) - L_0)/L_0) * 100$ . **c** A typical time evolution of temperature and strain. Temperature evolution is estimated assuming convective air cooling and estimated through a lumped-capacitance model, which gives  $T(t) = T_{\text{env}} + (T_0 - T_{\text{env}})e^{-t/\tau}$ ,  $T_{\text{env}}$ : room temperature,  $T_0$ : initial temperature of the sample,  $\tau$ : time variable of the system, defined by  $\tau = mc/(hA)$ ;  $m$ : mass of the sample,  $c$ : specific heat capacity,  $h$ : heat transfer coefficient,  $A$ : heat transfer surface area (see Supplementary Methods). **d** Snap shots of the deforming BMG in its supercooled liquid state. **e** Thickness distribution within the pulled wire.

cross section of the deforming sample and the strong temperature dependence of the viscosity control the evolution of temperature and strain rate profile (Fig. 1c). As the cross section of the sample continuously decreases, the cooling rate continuously increases (at least for  $T > T_g$ ). Strain rate ( $\dot{\gamma}$ ) under constant applied force is controlled by the time dependent cross-sectional area and by the temperature dependent viscosity. The latter can be approximated with a Vogel–Fulcher–Tammann (VFT) temperature dependence, hence exponentially increasing with decreasing temperature. Qualitatively  $\dot{\gamma}(T)$  exhibits a peak with values of several hundred strain per second, before decreasing again.

The samples which were processed according to the simultaneous cooling and straining processing protocol (Fig. 1) were subsequently characterized to determine their ductility (Fig. 2).

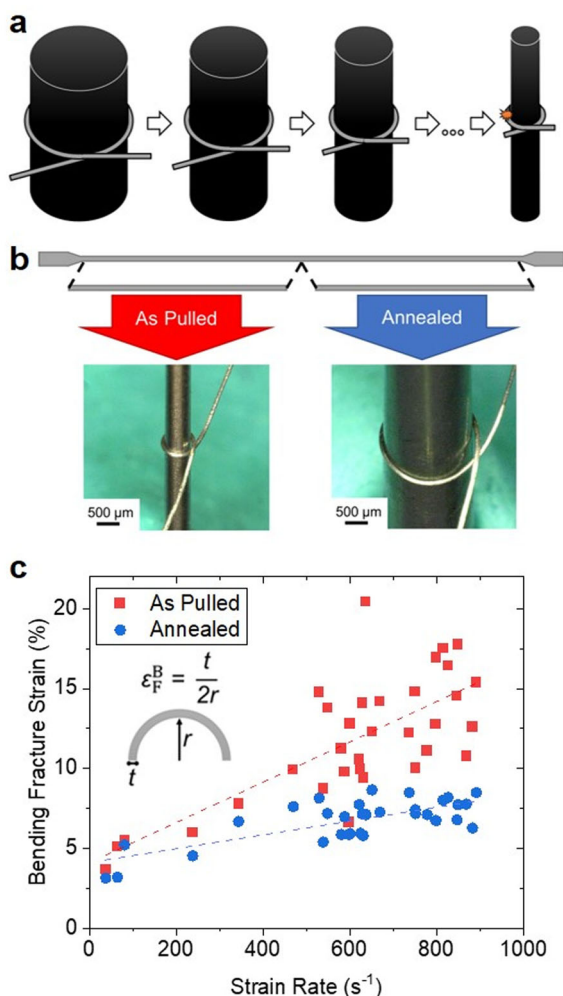


**Fig. 2** Characterization of the effect of excited liquid cooling on  $\text{Zr}_{44}\text{Ti}_{11}\text{Ni}_{10}\text{Cu}_{10}\text{Be}_{25}$  BMG bending ductility. **a** Wires are mechanically characterized through bending around cylinders of successively small diameter until fracture. **b** In order to separate the effects of excited liquid cooling from the fast cooling rate of the small geometry, wires are separated into two, with one segment characterized as pulled and the other annealed. **c** As pulled wires show a positive correlation between maximum strain rate of the pulling process and bending fracture strain. Annealed wires lose the added ductility to approximately the value of the as cast sample. However, as the final wire thickness decreases slightly with increasing strain rate, a small positive correlation between bending fracture strain and applied strain rate is present in the annealed wires, due to geometric effects in determining bending ductility<sup>34</sup>.

We choose bending characterization to determine the BMG samples' ductility. BMGs exhibit typically no ductility in tension<sup>8</sup>, and ductility measurements in compression are often overshadowed by misalignment and confinement effects<sup>32</sup>. Hardness and modulus trends have been associated with ductility trends and used for experimental convenience; however, these offer indirect information at best. The most reliable quantification of a ductile vs. brittle behavior can be achieved through fracture toughness measurements<sup>33</sup>. As those measurements are not possible due to the samples' geometry after pulling, we carry out bending experiments. It has been shown that some BMGs, including the  $\text{Zr}_{44}\text{Ti}_{11}\text{Ni}_{10}\text{Cu}_{10}\text{Be}_{25}$  alloy considered here, exhibit a well-defined and characteristic bending ductility in geometries where their thickness is below  $\sim 1$  mm<sup>34–36</sup>. As the absolute value of the bending ductility is a function of the samples' thickness<sup>34</sup>, only samples with similar thickness should be compared.

A summary of the bending characterization of the differently strained BMG samples is shown in Fig. 2. The bending fracture strain ( $\epsilon_F^B$ ) increases with increased experimental strain rate. For the same thickness of 100  $\mu\text{m}$ , the as-cast  $\text{Zr}_{44}\text{Ti}_{11}\text{Ni}_{10}\text{Cu}_{10}\text{Be}_{25}$  exhibits an average  $\epsilon_F^B = 6\%$ . With increasing strain rate,  $\epsilon_F^B$  increases from  $\sim 4\%$  for  $\dot{\gamma} \sim 40 \text{ s}^{-1}$  to a maximum value of  $\epsilon_F^B = 16\%$  for  $\dot{\gamma} = 890 \text{ s}^{-1}$ . In some cases, even higher plastic bending strains of up to  $\epsilon_F^B \sim 20\%$  are observed. We contribute the large scatter in the resulting bending fracture strain to the experimental difficulty of our setup in applying strain rate and cooling rate in a controlled synchronized way.

A challenge is to isolate the effect of the applied strain rate from other effects such as the cooling rate<sup>31</sup>. To be able to separate the effects, we annealed one half of each wire at  $T_g + 60$  K for 180 sec ( $\sim 500$  times the relaxation time<sup>37</sup>) to ensure that any history of the strain rate is erased after annealing, and a glass with the new fictive temperature of  $T_g + 60$  K is created while at this elevated temperature<sup>2</sup>. Cooling from  $T_g + 60$  K is carried out in the same way as the as-pulled samples, in ambient air, resulting in the same cooling rate as during the wire pulling experiments. Thereby, the history of the straining is erased in the annealed wires while maintaining the same cooling profile as in the as-pulled samples. Subtracting the property values of the annealed samples from those of the as-pulled samples allows us to isolate the effect of strain rate during excited liquid cooling on the ductility.

The samples that have been annealed after the pulling process exhibit a slightly higher but very similar  $\epsilon_F^B \sim 7\%$  compared to the as-cast material of  $\sim 6\%$ . This suggests that the significant enhancement in  $\epsilon_F^B$  measured in the as-pulled samples is predominantly due to the applied strain rate.

Thermal characterization was also carried out on samples processed through excited liquid cooling (Fig. 3). Specifically, we consider the enthalpy of relaxation,  $\Delta H_{\text{rel}}$ , which has been used as a thermodynamic measure to quantify the degree of rejuvenation<sup>27,38–41</sup>. For the strained samples, an increase in  $\Delta H_{\text{rel}}$  compare to the annealed sample is present (Fig. 3a). Specifically,  $\Delta H_{\text{rel}}$  increases from 0.21 kJ/mol for  $\dot{\gamma} = 215 \text{ s}^{-1}$  to 0.81 kJ/mol for the highest  $\dot{\gamma} = 830 \text{ s}^{-1}$  (Fig. 3b). The maximum absolute value of  $\Delta H_{\text{rel}}$  of 0.81 kJ/mol is comparable to previously reported sub  $T_g$  mechanical rejuvenation techniques including high pressure torsion and notched triaxial strain<sup>16,20,42</sup> and among the highest reported changes in enthalpy of relaxation when compared to the reference sample.

## Discussion

It has been widely shown that metallic glasses of the same chemistry can have greatly different ductility or fracture toughness<sup>43–45</sup>. Relative to the BMG's as-cast structure, ductility or fracture toughness can be reduced<sup>44,46,47</sup> or enhanced<sup>5,48</sup>. This can be

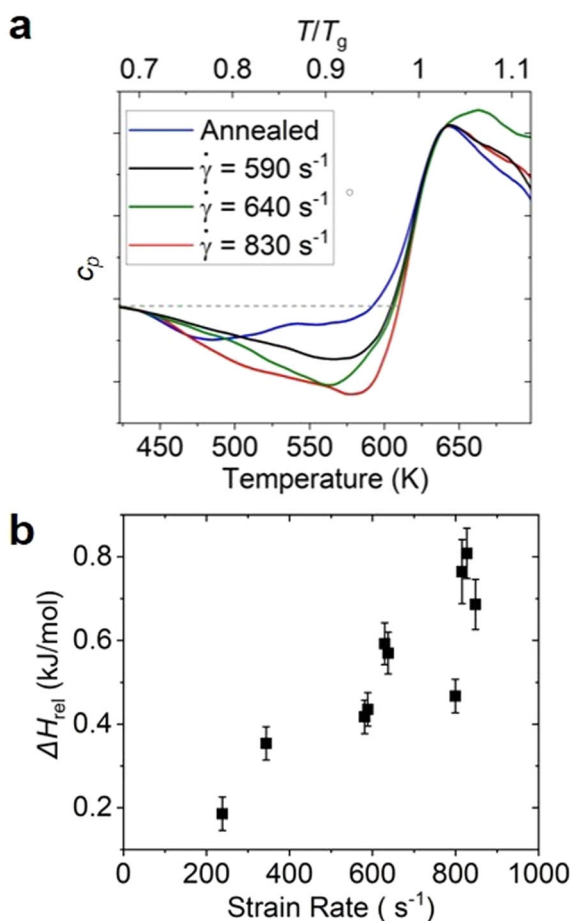


**Fig. 3 Thermal characterization of  $Zr_{44}Ti_{11}Ni_{10}Cu_{10}Be_{25}$  BMG processed through excited liquid cooling.** **a** Thermograms measured with differential scanning calorimetry reveal the thermal signal of the excited liquid cooling. **b** The enthalpy of relaxation increases with increasing strain rate applied during excited liquid cooling.

achieved through thermal treatments such as the use of different cooling rates<sup>5,41</sup>, annealing protocols<sup>2,40,46,49</sup>, or mechanical treatments such as quasistatic mechanical loading<sup>16–20</sup>, plastic deformation<sup>29,30,50,51</sup>, thermal cycling<sup>25–28</sup>, shot peening<sup>22</sup>, and radiation damage<sup>11–15</sup>. Whereas thermal treatments enable the liquid BMG former to be affected before it freezes into a glass, with mechanical treatments, the glass itself is manipulated. Manipulation of the glass is often inhomogeneous, most extremely during treatments that generate shear bands where most of the treatment effects are localized in shear bands occupying a very small volume fraction of the sample. The general understanding is that with both thermal and mechanical treatments, the potential energy of the glass can be manipulated. Enhancing the potential energy of a glass structure in the potential energy landscape is equivalent to increasing the fictive temperature of a glass<sup>52</sup>. Further, it has been argued that a high  $T_f$  can be generally associated with a larger ductility or fracture toughness<sup>2,5,48,53</sup>. The treatment of excited liquid cooling discussed here directly affects the supercooled liquid.

We argue that the straining of the supercooled liquid is counteracting the relaxation process, preventing the liquid from assuming its metastable equilibrium and hence causing it to assume an excited state (Fig. 4). The kinetic freezing of the (supercooled) liquid BMG former into a glass originates from the competition of the involved time scales. Under cooling conditions without an imposed strain rate, one of the involved time scales is set by the relaxation time,  $\tau_{rel}$ , which is the temperature

dependent time required for the liquid to assume the (meta)stable equilibrium configuration which continuously changes e.g., with temperature. Widely used to approximate  $\tau_{rel}$  is the VFT equation:  $\tau_{rel} = \tau_0 \exp\left(\frac{D^* T_0}{T - T_0}\right)$  with  $T_0$  as the VFT temperature,  $D^*$  the VFT fragility parameter, and  $\tau_0$  the high temperature limit of the relaxation time. This intrinsic time scale, with its exponential dependence on temperature, must be compared with the extrinsic time scale set by the processing protocol,  $\tau_{cool}$ . During a typical cooling process,  $\tau_{cool}$  is defined by the cooling rate,  $R$ , and can be described by  $\tau_{cool} = \frac{1}{R}$ . At high temperatures,  $\tau_{rel} < \tau_{cool}$ , and the liquid has sufficient time to reconfigure during cooling to its temperature dependent metastable equilibrium. At lower temperatures  $\tau_{rel} > \tau_{cool}$ , which is due to the exponential temperature dependence of  $\tau_{rel}$ , hence the liquid can no longer reconfigure into its temperature dependent metastable equilibrium. Consequently, the liquid falls out of metastable equilibrium at  $\tau_{rel} = \tau_{cool}$  and freezes into a glass. The temperature  $T_f$  at which this freezing occurs ( $\tau_{rel} = \tau_{cool}$ ) is referred to as the fictive temperature or the glass transition temperature upon cooling. As  $\tau_{rel}$  is an intrinsic property of the liquid BMG former, one is left with only  $\tau_{cool}$  as a tool to manipulate  $T_f$ . A higher cooling rate reduces  $\tau_{cool}$  and, hence, results in a glass with a higher fictive temperature (Fig. 4a).

In the present excited liquid cooling, a strain is applied at a certain rate during cooling of the liquid BMG former, working against the liquid's drive to assume a denser packed metastable equilibrium with decreasing temperatures. Straining a supercooled liquid BMG former causes it to dilate and loosens its packing<sup>54</sup>, which increases its potential energy in opposition to the relaxation process of decreasing potential energy with decreasing temperature. In order to assign a characteristic time to the straining process we assume a critical strain of 2% which results in a characteristic time,  $\tau_\gamma = \frac{0.02}{\dot{\gamma}}$ . Assuming 2% strain as a critical value to cause a “significant” structural change is based on previous work where this strain level has been observed to cause shear transformation zones to become unstable and cause a “significant” structural irreversible change<sup>55</sup>. However, it has also been pointed out that “weak” shear transformations occur at a much lower strain levels<sup>1,18,56,57</sup>, however significantly less in number.

When cooling a liquid BMG former under a strain rate, all three characteristic time scales,  $\tau_\gamma$ ,  $\tau_{rel}$ , and  $\tau_{cool}$  must be considered (Fig. 4). Following the liquid BMG former upon cooling, it remains in metastable equilibrium down to  $T_f^\gamma$  (Fig. 4). This is because for  $T > T_f^\gamma$  the time scales are such that  $\tau_{rel} < \tau_\gamma < \tau_{cool}$  hence, relaxation occurs within the available time. With decreasing temperature,  $\tau_{rel}$  increases and  $\tau_{rel} = \tau_\gamma$  at  $T = T_f^\gamma$ .

For temperatures below  $T_f^\gamma$ , the liquid can no longer reconfigure to reach its metastable equilibrium before that relaxation process is disturbed by the strain rate. Hence, the structure of the liquid falls out of metastable equilibrium and resumes an excited state characterized by  $T_f^\gamma$ . It is important to emphasize that the BMG is still in a liquid state, meaning that the structure rapidly changes, and these changes take place more rapidly than the available time set by the cooling rate  $\tau_{cool}$ . This “excited liquid” state which is present between  $T_f^\gamma$  and  $T_f$  is maintained through a competition between straining, which increases the potential energy, and relaxation, which decreases the potential energy. Upon further cooling  $\tau_{rel} = \tau_{cool}$  at  $T_f$  and the excited liquid is no longer able to reconfigure on the time scale set by the experiments and, consequently, freezes into an excited glass. Even though the excited liquid freezes into a glass at  $T_f$ , its structural state has been established at a higher temperature  $T_f^\gamma$  which is the



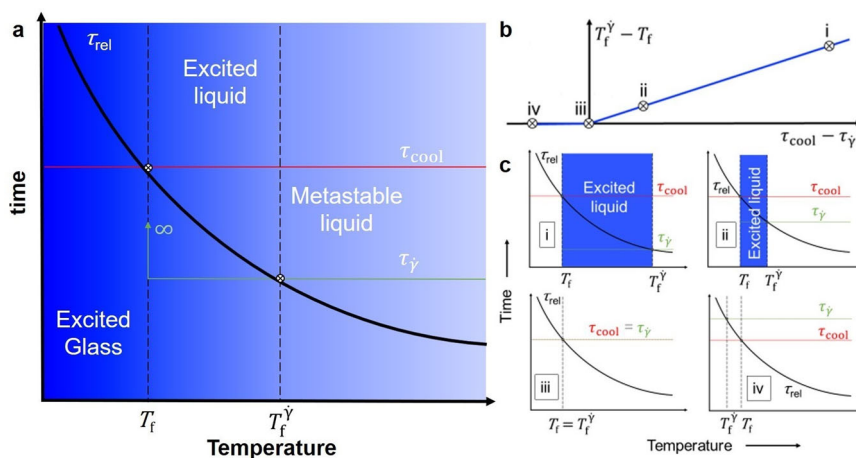


**Fig. 4 Excited liquid cooling mechanism.** **a** Illustration of the characteristic time scales involved in the excited liquid cooling mechanisms as a function of temperature. The structural relaxation time,  $\tau_{rel}$ , increases exponentially with decreasing temperature (black curve). A requirement for the excited liquid cooling mechanism is that the time scale set by the strain rate (green line),  $\tau_{\dot{\gamma}} = \frac{0.02}{\dot{\gamma}}$  is smaller than the available time set by the cooling rate (red line),  $\tau_{cool} = \frac{1}{R}$ . Upon cooling, the liquid BMG former remains in metastable equilibrium for  $\tau_{rel} < \tau_{\dot{\gamma}}$  until  $\tau_{rel} = \tau_{\dot{\gamma}}$ . Here, an “excited liquid” state is maintained through a competition between straining, causing the potential energy to increase, and relaxation, which decreases the potential energy for  $T_f^{\dot{\gamma}} > T > T_f$  ( $\dot{\gamma} = 0$ ). When  $\tau_{rel} = \tau_{cool}$ , at  $T_f$ , the excited liquid can no longer reconfigure on the experimental time scale to maintain its metastable equilibrium and freezes into an excited glass. The structure that freezes into a glass at  $T_f$  is that of the excited liquid with a fictive temperature of  $T_f^{\dot{\gamma}}$ . **b, c** The effectiveness of excited liquid cooling is controlled by the relative rates of cooling and straining, inversely related to  $\tau_{cool}$  and  $\tau_{\dot{\gamma}}$ . For  $\tau_{cool} - \tau_{\dot{\gamma}} > 0$ , the enhancement of fictive temperature  $T_f^{\dot{\gamma}} - T_f$  scales with  $\tau_{cool} - \tau_{\dot{\gamma}}$  (i and ii). For  $\tau_{cool} - \tau_{\dot{\gamma}} \leq 0$ , structural rearrangements due to  $\dot{\gamma}$  do not occur (sufficiently) and hence do not affect fictive temperature or ductility (iii and iv).

underlying mechanism of the excited liquid cooling method to achieve a ductile glass.

The effect of an applied strain rate in excited liquid cooling on increasing the fictive temperature of the glass (and hence ductility) depends on the relative magnitudes of the characteristic time scales. To increase the fictive temperature through an application of a strain rate, meaning  $T_f^{\dot{\gamma}} > T_f$  ( $\dot{\gamma} = 0$ ) requires  $\tau_{\dot{\gamma}} < \tau_{cool}$ . If  $\tau_{\dot{\gamma}} > \tau_{cool}$ , the time required for structural changes to occur due to straining exceeds the time available during the cooling process and hence, structural changes originating from an applied strain rate do not occur. For example, a strain rate  $> 2 \text{ s}^{-1}$  is required to enhance the fictive temperature and thereby ductility during bulk metallic glass formation at a cooling rate of 100 K/s ( $\tau_{cool} = 10^{-2} \text{ s}$ ). The effectiveness of  $\dot{\gamma}$  in enhancing fictive temperature scales with  $\tau_{cool} - \tau_{\dot{\gamma}}$  (Fig. 4b, c). For  $\tau_{cool} - \tau_{\dot{\gamma}} > 0$ , the enhancement of fictive temperature  $T_f^{\dot{\gamma}} - T_f$  scales with  $\tau_{cool} - \tau_{\dot{\gamma}}$ . With decreasing strain rate (but the same cooling rate) such that  $\tau_{cool} - \tau_{\dot{\gamma}} \leq 0$ , structural rearrangements due to  $\dot{\gamma}$  can no longer significantly occur on the time scale of experiment. Hence, it is only for combinations of strain rates and cooling rates that fulfill  $\tau_{cool} - \tau_{\dot{\gamma}} > 0$  that excited liquid cooling takes place. The effect on ductility increases with increasing  $\tau_{cool} - \tau_{\dot{\gamma}}$ .

In the proposed mechanism for excited liquid cooling assumptions where made which will now be discussed. Key to excited liquid cooling is the competition between relaxation and straining. Relaxation is a three-dimensional mechanism where atoms under the action of thermal energy (quantified in temperature) probe a vast range of structural states. On the other hand, the strain rate applied here is a one-dimensional mechanism which may even result in anisotropic properties and structure<sup>58,59</sup>. During excited liquid cooling, the two effects compete with each other. However, structural relaxation is a more efficient mechanism utilizing all three physical dimensions to lower potential energy whereas strain rate only meaningfully accesses one dimension to increase potential energy. This makes a quantitative comparison of both contributions challenging.

Furthermore, in the above discussion on the mechanism of excited liquid cooling, we assumed a constant applied strain rate down to  $T = T_f$ . In general, such an assumption is oversimplified. Fundamentally, metallic glasses change their deformation behavior as a function of temperature and strain rate. At high temperatures, they deform in a homogenous fashion, essentially entirely affine, whereas at low temperatures, deformation is highly localized and non-affine<sup>60</sup>. To qualitatively represent this dramatic change in behavior as a function of temperature we assume  $\dot{\gamma} = const \geq 0$  as a finite and constant strain rate for  $T > T_f$  and  $\dot{\gamma} = 0$  for  $T < T_f$ . This behavior is however simplified, as the practically realizable changes in  $\dot{\gamma}(T)$  between  $T_1$  and  $T_f$  are less drastic.

It is generally understood that the viscosity in BMG forming liquids for  $T > T_f$  is strain rate independent<sup>61,62</sup>. However, for high strain rates, significant non-Newtonian effects have been observed<sup>63–65</sup>, which may also take place during excited liquid cooling. In addition, straining of the sample may also generate heat which will affect cooling rate. Considering all this, our model to describe excited liquid cooling under the current assumptions offers only a qualitative description. For a quantitative description, more complicated calculations, using more detailed values of evolving process variables, would be required.

To compare the effectiveness of excited liquid cooling with other BMG rejuvenation methods, we use the enthalpy of relaxation,  $\Delta H_{rel}$ , which has been reported in most publications on rejuvenation techniques (Supplementary Table 1). Comparison reveals that excited liquid cooling is among the most effective techniques to enhance the potential energy of the glass, offering a considerable increase in the enthalpy of relaxation through a mechanism directly affecting the liquid. It should be mentioned that comparison of these techniques by their effects on mechanical properties is not possible, as the reported studies of the various methods use different properties.

The technological motivation of the various techniques to rejuvenate metallic glasses is to improve mechanical properties<sup>10,25–27</sup>. Therefore, such methods, including our excited

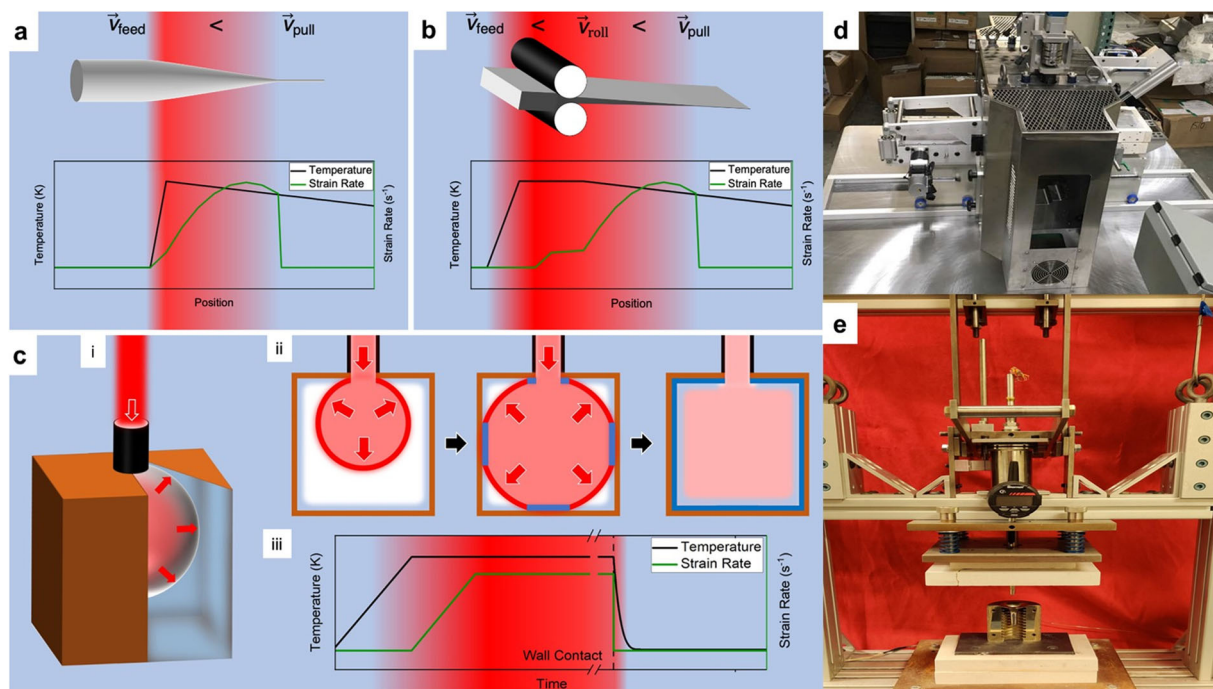


**Fig. 5 BMG processing techniques that can be extended to incorporate excited liquid cooling.** **a** Wire pulling where the wire ductility is controlled through maximizing  $T_f^y - T_f$ . For a given strain rate,  $T_f^y - T_f$  scales with the steepness of the spatial temperature gradient (From bright red being the highest temperature to blue being any temperature below  $T_f$ ). **b** In order to fabricate ductile sheets, excited liquid cooling can be realized through hot-rolling and subsequent pulling of the escaping sheet down a temperature gradient. **c** Blow molding<sup>66</sup> against a cold mold results into excited liquid cooling and hence enables to net-shape BMG articles into their ductile state. **d** A hot-rolling mill with a puller to realize **b**. **e** A blow-molding machine to realize **c**.

liquid cooling, will have to be practical to be used as a toughening strategy for metallic glass articles. Key to an effective practical usage of the excited liquid cooling method is a sufficiently high strain rate ( $\tau_{cool} - \tau_y > 0$ ) present at temperatures including  $T_f$  and  $T_f^y$ , and that the excited liquid can be frozen into a glass state. It is important to mention that the absolute strain applied during excited liquid cooling is irrelevant. In the present setup, we use such high strains only for experimental convenience. To generate and freeze an excited liquid, only the strain rate over a narrow temperature interval is relevant. This interval is in the vicinity of  $T_f$ , where it sets  $T_f^y$  and maintains this state until  $T_f$ . Such a situation can be realized in several metallic glass fabrication methods (Fig. 5). For example, the pulling used here can be utilized to fabricate ductile metallic glass wires as a final product (Fig. 5a). Similarly, sheets can be produced. For their synthesis, in addition to regular rolling, a subsequent pulling of the escaping sheet is required to establish a simultaneous straining and cooling. If one establishes  $\tau_{cool} - \tau_y > 0$  for temperatures down to  $T_f$ , ductile sheets can be fabricated (Fig. 5b, d). The requirement of  $\tau_{cool} - \tau_y > 0$  for temperatures down to  $T_f$  can also be realized during blow molding and thereby net-shape complex BMG articles while establishing their ductile state (Fig. 5c, e). Here, the BMG feedstock is deformed through a gas pressure towards a cold mold. It has been previously determined that once the BMG touches the mold, the strain rate drops essentially instantaneous to zero<sup>66,67</sup>. If the mold is set to a low temperature, and a temperature gradient between deforming feedstock and mold can be established through the separating vacuum, the excited liquid can be rapidly frozen into a glass upon touching the mold, hence BMGs parts can be net-shaped into their ductile state.

**Conclusion.** In summary, we show here that an applied strain rate can excite the BMG in its liquid state to a higher potential energy. Microscopically, straining causes the structure to dilate,

hence “pulls” the structure energetically up the potential energy landscape. Upon further cooling, the resulting excited liquid freezes into an excited glass that can triple its ductility compared to that of the unstrained material. Based on the requirement for the excited liquid cooling, we identify metallic glass processing techniques that allow to shape and net-shape metallic glasses into a complex geometry while assuming a ductile state.

## Methods

**Sample preparation.** The amorphous  $Zr_{44}Ti_{11}Ni_{10}Cu_{10}Be_{25}$  rods of  $\sim 1.8$  mm in diameter were prepared by copper mold casting. High purity ingots (for all constituent purity higher than 99.99) were arc-melted under argon atmosphere to alloy the constituents. Subsequently, the alloy was reheated to a temperature of  $\sim 1000$  °C and under an argon gas pressure forced from the quartz nozzle into a copper mold. Thermal analysis on some of the rods reveal the typical thermogram for a fully amorphous sample which was cooled with a rate  $\sim 500$  K/sec<sup>2</sup>.

**Thermal analysis.** Thermal analysis was conducted using in a TA Q200 differential scanning calorimeter under argon flow with a heating rate of  $20$  K min<sup>-1</sup>. All samples were heated through crystallization, subsequently cooled, and then heated again with the same heating rate to establish a baseline to be subtracted from the initial heating run. Measurements for the enthalpy of relaxation were made by finding the area of the curve with respect to the baseline, shown as a dashed line in Fig. 3a.

**Strain rate.** Sample rod is held from above inside an RF-coil, affixed with a hanging weight (100 g) and a second weight that is suspended so as to not exert any force on the sample initially (0–10,000 g). The RF-coil is turned on, and once the rod deforms sufficiently to lengthen 5mm due to the 100 g force, the larger weight is released and rapidly strains the sample rod into a wire. Strain rate is determined from video analysis and varied by changing the mass of the second weight. The first processing step with the 100 g weight warrants control over the initial temperature as the deformation to 5 mm is predominately controlled by viscosity which is highly temperature sensitive<sup>37</sup> (Supplementary Figure 1). Strain rate is controlled through the use of different weights.

**Bending characterization.** Wires are divided into roughly equal segments and separated into two categories: as pulled and annealed. Annealed wires are subjected to a treatment described in Supplementary Fig. 2. Both sets of wires are

characterized via bending around cylinders of successively smaller diameters until fracture (Fig. 2). Fractured wires are measured under an optical microscope to determine thickness and radius of fracture to determine bending plastic strain. This value is then added to the measured elastic strain limit (which is in close agreement with previously reported values<sup>55</sup>) to determine bending fracture strain  $\epsilon_B^B$ .

### Data availability

The raw data generated during this study are available from the corresponding author on reasonable request.

Received: 30 October 2020; Accepted: 31 January 2021;

Published online: 26 February 2021

### References

- Fan, Y., Iwashita, T. & Egami, T. How thermally activated deformation starts in metallic glass. *Nat. Commun.* **5**, 5083 (2014).
- Ketkaew, J. et al. Mechanical glass transition revealed by the fracture toughness of metallic glasses. *Nat. Commun.* **9**, <https://doi.org/10.1038/s41467-018-05682-8> (2018).
- Ketkaew, J., Fan, M., Shattuck, M. D., O'Hern, C. S. & Schroers, J. Structural relaxation kinetics defines embrittlement in metallic glasses. *Scripta Mater.* **149**, 21–25 (2018).
- Fan, Y., Iwashita, T. & Egami, T. Crossover from localized to cascade relaxations in metallic glasses. *Phys. Rev. Lett.* **115**, 045501 (2015).
- Fan, M. et al. Effects of cooling rate on particle rearrangement statistics: rapidly cooled glasses are more ductile and less reversible. *Phys. Rev. E* **95**, 022611 (2017).
- Ashwin, J., Bouchbinder, E. & Procaccia, I. Cooling-rate dependence of the shear modulus of amorphous solids. *Phys. Rev. E* **87**, 042310 (2013).
- Ashby, M. F. & Greer, A. L. Metallic glasses as structural materials. *Scripta Mater.* **54**, 321–326 (2006).
- Schuh, C. A., Hufnagel, T. C. & Ramamurty, U. Overview No.144 - Mechanical behavior of amorphous alloys. *Acta Mater.* **55**, 4067–4109 (2007).
- Shao, L. et al. Effect of chemical composition on the fracture toughness of bulk metallic glasses. *Materialia* **12**, 10082810.1016/j.mtla.2020.100828 (2020).
- Sun, Y. H., Concustell, A. & Greer, A. L. Thermomechanical processing of metallic glasses: extending the range of the glassy state. *Nat. Rev. Mater.* **1**, 1603910.1038/natrevmats.2016.39 (2016).
- Baumer, R. E. & Demkowicz, M. J. Radiation response of amorphous metal alloys: Subcascades, thermal spikes and super-quenched zones. *Acta Mater.* **83**, 419–430 (2015).
- Raghavan, R. et al. Ion irradiation enhances the mechanical performance of metallic glasses. *Scripta Mater.* **62**, 462–465 (2010).
- Magagnosc, D. J. et al. Effect of ion irradiation on tensile ductility, strength and fictive temperature in metallic glass nanowires. *Acta Mater.* **74**, 165–182 (2014).
- Ebner, C., Rajagopalan, J., Lekka, C. & Rentenberger, C. Electron beam induced rejuvenation in a metallic glass film during in-situ TEM tensile straining. *Acta Mater.* **181**, 148–159 (2019).
- Sun, K. et al. Structural rejuvenation and relaxation of a metallic glass induced by ion irradiation. *Scripta Mater.* **180**, 34–39 (2020).
- Pan, J. et al. Extreme rejuvenation and softening in a bulk metallic glass. *Nat. Commun.* **9**, 560 (2018).
- Park, K. W. et al. Elastostatically induced structural disordering in amorphous alloys. *Acta Mater.* **56**, 5440–5450 (2008).
- Ju, J. D., Jang, D., Nwankpa, A. & Atzmon, M. An atomically quantized hierarchy of shear transformation zones in a metallic glass. *J. Appl. Phys.* **109**, 053522 (2011).
- Ju, J. D. & Atzmon, M. A comprehensive atomistic analysis of the experimental dynamic-mechanical response of a metallic glass. *Acta Mater.* **74**, 183–188 (2014).
- Pan, J., Ivanov, Y. P., Zhou, W. H., Li, Y. & Greer, A. L. Strain-hardening and suppression of shear-banding in rejuvenated bulk metallic glass. *Nature* **578**, 559–562 (2020).
- Packard, C. E., Witmer, L. M. & Schuh, C. A. Hardening of a metallic glass during cyclic loading in the elastic range. *Appl. Phys. Lett.* **92**, 171911 (2008).
- Concustell, A., Mear, F. O., Surinach, S., Baro, M. D. & Greer, A. L. Structural relaxation and rejuvenation in a metallic glass induced by shot-peening. *Phil. Mag. Lett.* **89**, 831–840 (2009).
- Lee, M. H. et al. Improved plasticity of bulk metallic glasses upon cold rolling. *Scripta Mater.* **62**, 678–681 (2010).
- Zhang, L. et al. Rejuvenated metallic glass strips produced via twin-roll casting. *J. Mater. Sci. Technol.* **38**, 73–79 (2020).
- Ketov, S. V. et al. Rejuvenation of metallic glasses by non-affine thermal strain. *Nature* **524**, 200–203 (2015).
- Li, B. S., Xie, S. H. & Kruzic, J. J. Toughness enhancement and heterogeneous softening of a cryogenically cycled Zr-Cu-Ni-Al-Nb bulk metallic glass. *Acta Mater.* **176**, 278–288 (2019).
- Ketkaew, J. et al. The effect of thermal cycling on the fracture toughness of metallic glasses. *Acta Mater.* **184**, 100–108 (2020).
- Das, A., Dufresne, E. M. & Maass, R. Structural dynamics and rejuvenation during cryogenic cycling in a Zr-based metallic glass. *Acta Mater.* **196**, 723–732 (2020).
- Dmowski, W. et al. Structural rejuvenation in a bulk metallic glass induced by severe plastic deformation. *Acta Mater.* **58**, 429–438 (2010).
- Wang, X. D. et al. Atomic-level structural modifications induced by severe plastic shear deformation in bulk metallic glasses. *Scripta Mater.* **64**, 81–84 (2011).
- Dong, J. et al. Rejuvenation in hot-drawn micrometer metallic glassy wires. *Chinese Phys. Lett.* **37**, 017103 (2020).
- Wu, W. F., Li, Y. & Schuh, C. A. Strength, plasticity and brittleness of bulk metallic glasses under compression: statistical and geometric effects. *Philos. Mag.* **88**, 71–89 (2008).
- Lewandowski, J. J., Wang, W. H. & Greer, A. L. Intrinsic plasticity or brittleness of metallic glasses. *Phil. Mag. Lett.* **85**, 77–87 (2005).
- Conner, R. D., Johnson, W. L., Paton, N. E. & Nix, W. D. Shear bands and cracking of metallic glass plates in bending. *J. Appl. Phys.* **94**, 904–911 (2003).
- Chen, W. et al. Test sample geometry for fracture toughness measurements of bulk metallic glasses. *Acta Mater.* **145**, 477–487 (2018).
- Nollmann, N., Binkowski, I., Schmidt, V., Rosner, H. & Wilde, G. Impact of micro-alloying on the plasticity of Pd-based bulk metallic glasses. *Scripta Mater.* **111**, 119–122 (2016).
- Gallino, I., Schroers, J. & Busch, R. Kinetic and thermodynamic studies of the fragility of bulk metallic glass forming liquids. *J. Appl. Phys.* **108**, 063501 (2010).
- Cangialosi, D. Dynamics and thermodynamics of polymer glasses. *J. Phys. Condens. Mater.* **26**, 153101 (2014).
- Wakeda, M., Saida, J., Li, J. & Ogata, S. Controlled rejuvenation of amorphous metals with thermal processing. *Sci. Rep.* **5**, 10545 (2015).
- Guo, W., Saida, J., Zhao, M., Lu, S. L. & Wu, S. S. Thermal rejuvenation of an Mg-based metallic glass. *Metall. Mater. Trans. A* **50a**, 1125–1129 (2019).
- Saida, J., Yamada, R., Wakeda, M. & Ogata, S. Thermal rejuvenation in metallic glasses. *Sci. Technol. Adv. Mater.* **18**, 152–162 (2017).
- Meng, F., Tsuchiya, K., Seiichiro, I. & Yokoyama, Y. Reversible transition of deformation mode by structural rejuvenation and relaxation in bulk metallic glass. *Appl. Phys. Lett.* **101**, 121914 (2012).
- Wu, T. W. & Spaepen, F. The relation between embrittlement and structural relaxation of an amorphous metal. *Philos. Mag.* **61**, 739–750 (1990).
- Gilbert, C. J., Ritchie, R. O. & Johnson, W. L. Fracture toughness and fatigue-crack propagation in a Zr-Ti-Ni-Cu-Be bulk metallic glass. *Appl. Phys. Lett.* **71**, 476–478 (1997).
- Rycroft, C. H. & Bouchbinder, E. Fracture toughness of metallic glasses: annealing-induced embrittlement. *Phys. Rev. Lett.* **109**, 194301 (2012).
- Wu, T. W. & Spaepen, F. Embrittlement of metallic glasses. *J. Metals* **36**, 54–54 (1984).
- Pampillo, C. A. & Polk, D. E. Annealing embrittlement in an iron-nickel-based metallic glass. *Mater. Sci. Eng.* **33**, 275–280 (1978).
- Louzuigne-Luzgin, D. V., Saito, T., Saida, J. & Inoue, A. Influence of cooling rate on the structure and properties of a Cu-Zr-Ti-Ag glassy alloy. *J. Mater. Res.* **23**, 515–522 (2008).
- Murah, P. & Ramamurty, U. Embrittlement of a bulk metallic glass due to sub-T-g annealing. *Acta Mater.* **53**, 1467–1478 (2005).
- Zhou, H. B., Hubek, R., Peterlechner, M. & Wilde, G. Two-stage rejuvenation and the correlation between rejuvenation behavior and the boson heat capacity peak of a bulk metallic glass. *Acta Mater.* **179**, 308–316 (2019).
- Ryu, W., Yamada, R. & Saida, J. Tailored hardening of ZrCuAl bulk metallic glass induced by 2D gradient rejuvenation. *Npg Asia Mater* **12**, 52 (2020).
- Debenedetti, P. G., Stillinger, F. H. & Shell, M. S. Model energy landscapes. *J. Phys. Chem. B* **107**, 14434–14442 (2003).
- Shen, J., Huang, Y. J. & Sun, J. F. Plasticity of a TiCu-based bulk metallic glass: effect of cooling rate. *J. Mater. Res.* **22**, 3067–3074 (2007).
- Spaepen, F. Metallic glasses: must shear bands be hot? *Nat. Mater.* **5**, 7–8 (2006).
- Johnson, W. L. & Samwer, K. A universal criterion for plastic yielding of metallic glasses with a (T/T-g)(2/3) temperature dependence. *Phys. Rev. Lett.* **95**, 195501 (2005).
- Atzmon, M. & Ju, J. D. Microscopic description of flow defects and relaxation in metallic glasses. *Phys. Rev. E* **90**, 042313 (2014).
- Fan, M., Zhang, K., Schroers, J., Shattuck, M. D. & O'Hern, C. S. Particle rearrangement and softening contributions to the nonlinear mechanical response of glasses. *Phys. Rev. E* **96**, 032602 (2017).



58. Sun, Y. et al. Flow-induced elastic anisotropy of metallic glasses. *Acta Mater.* **112**, 132–140 (2016).
59. Wu, B., Iwashita, T. & Egami, T. Anisotropy of stress correlation in two-dimensional liquids and a pseudospin model. *Phys. Rev. E* **92**, 052303 (2015).
60. Spaepen, F. Microscopic mechanism for steady-state inhomogeneous flow in metallic glasses. *Acta Metall. Mater.* **25**, 407–415 (1977).
61. Kawamura, Y. & Inoue, A. Newtonian viscosity of supercooled liquid in a Pd<sub>40</sub>Ni<sub>40</sub>P<sub>20</sub> metallic glass. *Appl. Phys. Lett.* **77**, 1114–1116 (2000).
62. Lu, J., Ravichandran, G. & Johnson, W. L. Deformation behavior of the Zr<sub>41.2</sub>Ti<sub>13.8</sub>Cu<sub>12.5</sub>Ni<sub>10</sub>Be<sub>22.5</sub> bulk metallic glass over a wide range of strain-rates and temperatures. *Acta Mater.* **51**, 3429–3443 (2003).
63. Lohwongwatana, B., Schroers, J. & Johnson, W. L. Strain rate induced crystallization in bulk metallic glass-forming liquid. *Phys. Rev. Lett.* **96**, 075503 (2006).
64. Langer, J. S. & Egami, T. Glass dynamics at high strain rates. *Phys. Rev. E* **86**, 011502 (2012).
65. Shao, Z. et al. Shear-accelerated crystallization in a supercooled atomic liquid. *Phys. Rev. E* **91**, 020301 (2015).
66. Schroers, J. et al. Thermoplastic blow molding of metals. *Mater. Today* **14**, 14–19 (2011).
67. Mota, R. M. O. et al. Overcoming geometric limitations in metallic glasses through stretch blow molding. *Appl. Mater. Today* **19**, 100567 (2020).

### Acknowledgements

This research was supported by the Office of Naval Research under grant N00014-20-1-2200. The authors also thank Eran Bouchbinder for insightful discussions. R.O. thanks Consejo Nacional de Ciencia y Tecnología and Secretaría de Energía (CONACYT-SENER) for the financial support provided in the pursuit of his doctoral studies. D.J.B. is grateful for University College Dublin support for research sabbatical at Yale University, 2019–2020.

### Author contributions

J.S. conceived and supervised the project. R.O. and E.L. contributed equally to this work, with the project ideation, designing the testing setup, preparing samples, performing

measurements and relevant calculations. A.W., S.C. and D.C.H. were involved in the feasibility and initial ideation. D.J.B. and S.S. contributed with the initial experiments and project execution discussions. J.S., R.O. and E.L. wrote the initial draft of the paper. All authors contributed to the discussion and finishing of the final paper.

### Competing interests

The authors declare no competing interests.

### Additional information

**Supplementary information** The online version contains supplementary material available at <https://doi.org/10.1038/s43246-021-00127-0>.

**Correspondence** and requests for materials should be addressed to J.S.

**Reprints and permission information** is available at <http://www.nature.com/reprints>

**Publisher's note** Springer Nature remains neutral with regard to jurisdictional claims in published maps and institutional affiliations.



**Open Access** This article is licensed under a Creative Commons Attribution 4.0 International License, which permits use, sharing, adaptation, distribution and reproduction in any medium or format, as long as you give appropriate credit to the original author(s) and the source, provide a link to the Creative Commons license, and indicate if changes were made. The images or other third party material in this article are included in the article's Creative Commons license, unless indicated otherwise in a credit line to the material. If material is not included in the article's Creative Commons license and your intended use is not permitted by statutory regulation or exceeds the permitted use, you will need to obtain permission directly from the copyright holder. To view a copy of this license, visit <http://creativecommons.org/licenses/by/4.0/>.

© The Author(s) 2021